Numer. Math. Theor. Meth. Appl.
doi: 10.4208/nmtma.OA-2025-0043

Vol. **19**, No. 1, pp. 80-105
February 2026

A Gradient Recovery Technique for Enhancing the Convergence of Demagnetizing Field Based on PDE Approach

Jing Wu[1], Zixuan Cui[2], Lei Yang[2,3] and Guanghui Hu[4,5,*]

[1] *School of Mathematical Sciences, Soochow University, Suzhou 215006, China*
[2] *School of Computer Science and Engineering, Macau University of Science and Technology, Macau SAR 999078, China*
[3] *Macau University of Science and Technology Zhuhai MUST Science and Technology Research Institute, Zhuhai 519031, China*
[4] *State Key Laboratory of Internet of Things for Smart City and Department of Mathematics, University of Macau, Macau SAR 999078, China*
[5] *Zhuhai UM Science & Technology Research Institute, Zhuhai 519031, China*

Received 27 April 2025; Accepted (in revised version) 3 September 2025

Abstract. The PDE approach is a popular technique for the demagnetizing field calculation due to the flexibility in handling complex domains. However, it faces a challenge on delivering desired accuracy due to the suboptimal convergence of the function gradient and singularity on the boundary. In this work, a robust gradient recovery technique is applied and analysed for fixing such an issue. An L^2 error estimate of the finite element approximation for the demagnetizing field is derived, which consists of two parts, i.e., of finite element discretization error and boundary approximation error. A gradient recovery method based on the polynomial preserving recovery technique is applied to enhance the accuracy of the finite element approximation, and a superconvergence result is established. An idea of locally refined surface meshes is applied to resolve the singularity in the boundary conditions, thereby reducing boundary approximation errors. Extensive numerical tests are provided to verify our theoretical findings and the efficiency of our proposed method. The results indicate that the proposed method achieves second-order convergence for the approximate demagnetizing field, positioning it as a highly competitive technique to develop optimal algorithms in computational micromagnetics.

AMS subject classifications: 65N12, 65N15, 65N30

Key words: Demagnetizing field, PDE approach, finite element method, gradient recovery technique, polynomial preserving recovery method, superconvergence.

*Corresponding author. *Email addresses:* jwu02@outlook.com (J. Wu), 3220003539@student.must.edu.mo (Z. Cui), leiyang@must.edu.mo (L. Yang), garyhu@um.edu.mo (G. Hu)

1. Introduction

Computational micromagnetics has been playing a significant role in several applications, including new data storage, hyper-sound speakers, and neuronal simulations [6, 12, 17, 18]. A fundamental governing equation of micromagnetics is the following Landau-Lifshitz-Gilbert equation:

$$\frac{\partial}{\partial t}\vec{\mathrm{M}} = -\gamma_G \vec{\mathrm{M}} \times \vec{\mathrm{H}}_{eff} + \frac{\alpha}{\vec{\mathrm{M}}_s}\vec{\mathrm{M}} \times \frac{\partial}{\partial t}\vec{\mathrm{M}},$$

where $\vec{\mathrm{M}}$ is the magnetization, $\vec{\mathrm{M}}_s$ is the saturation magnetization, γ_G is the Gilbert gyromagnetic ratio, α is the dimensionless damping coefficient, and $\vec{\mathrm{H}}_{eff}$ is the effective field. The effective field is composed of exchange field, anisotropy field, external field, and the demagnetizing field, where the demagnetizing field ($\vec{\mathrm{H}}_{dem}$) is given by the following equation and its calculation is very challenging [2, 19, 24, 28, 29]:

$$\vec{\mathrm{H}}_{dem}(\vec{x}) = -\nabla\phi(\vec{x}), \quad \phi(\vec{x}) = \frac{1}{4\pi}\int_\Omega \vec{\mathrm{M}}(\vec{x}') \cdot \nabla_{\vec{x}'}\left(\frac{1}{|\vec{x}-\vec{x}'|}\right) d\vec{x}', \tag{1.1}$$

where Ω is a bounded domain with Lipschitz and piecewise smooth boundary $\partial\Omega$.

It is known that the direct calculation of the demagnetizing field using (1.1) will cause $\mathcal{O}(N^2)$ computational complexity, where N denotes the total amount of the mesh nodes. In order to reduce the computational complexity, a variety of approaches have been developed for the demagnetizing field calculation, including the fast Fourier transform (FFT) method [2, 19], the fast multipole method (FMM) [3, 4], and the PDE approach [15, 28, 29]. The PDE approach is popular for its flexibility in handling complex domains and advantage in computational complexity. In this approach, the potential $\phi(\vec{x})$ is split into two parts, i.e., $\phi = \phi_1 + \phi_2$, where ϕ_1 and ϕ_2 are successively calculated by the following two Poisson equations:

$$\begin{cases} \nabla^2\phi_1(\vec{x}) = \nabla \cdot \vec{\mathrm{M}}(\vec{x}) & \text{in } \Omega, \\ \phi_1 = 0 & \text{on } \partial\Omega, \end{cases} \tag{1.2}$$

$$\begin{cases} \nabla^2\phi_2(\vec{x}) = 0 & \text{in } \Omega, \\ \phi_2(\vec{x}) = g(\vec{x}) := \displaystyle\int_{\partial\Omega} N(\vec{x}-\vec{y})\left(\vec{\mathrm{M}}\cdot\vec{n} + \frac{\partial\phi_1}{\partial\vec{n}}\right) d\vec{y} & \text{on } \partial\Omega, \end{cases} \tag{1.3}$$

where $N(\vec{x}-\vec{y}) = -1/(4\pi|\vec{x}-\vec{y}|)$ is the Newtonian potential. Once ϕ is obtained, the demagnetizing field $\vec{H}_{dem}$ is calculated by taking the negative gradient of it, i.e., $\vec{H}_{dem} = -\nabla\phi$, and then the following demagnetizing field energy which is important in practice can be obtained:

$$\vec{E}_{dem} = -\frac{\mu_0}{2}\int_\Omega \vec{\mathrm{H}}_{dem} \cdot \vec{\mathrm{M}} d\vec{x} = \frac{\mu_0}{2}\int_\Omega |\nabla\phi(\vec{x})|^2 d\vec{x},$$

where μ_0 is the magnetic permeability of the vacuum.

This approach changes the integral representation of the boundary contribution from a double-layer potential to a single-layer potential (1.3) which has less singularity and therefore can be handled numerically more easily. In this approach, the evaluation of the integral is transferred into solving two PDEs, for which the finite element method (FEM) is a competitive candidate for its mature theory and algorithms. The accurate calculation is a non-trivial challenge for the calculation of the demagnetizing field, because, on the one hand, the gradient of the finite element solution loses an order of accuracy [10], and on the other hand, the singularity in the surface integral g has to be treated carefully. However, evidence suggests that the former numerical issue has received limited attention in the existing literature [1, 14, 16, 25, 26]. Although Schrefl [25] recognized the loss of gradient accuracy and attempted to compensate for this by employing quadratic elements to improve the convergence order, this approach fundamentally differs from recovering the gradient. Therefore, it is essential to improve the accuracy of the gradient by some gradient recovery post-processing techniques. Recently, Hu *et al.* [28] considered the PDE approach combining the linear FEM with the superconvergence patch recovery (SPR) technique [30]. The numerical experiments demonstrate that this methodology achieves higher-order approximation of $\nabla\phi$, thereby enhancing the demagnetizing field calculation accuracy, while the theoretical verification remains open.

Another popular gradient recovery technique is the polynomial preserving recovery (PPR) method, proposed by Zhang and Naga [22] has been incorporated into commercial software such as ANSYS, Abaqus, COMSOL Multiphysics. The PPR technique recovers the gradient by local least-squares fitting directly to the finite element solution, rather than utilizing its gradient as in the SPR approach. The PPR technique preserves the polynomial of degrees one more than the order of the FEM, resulting in a more robust theoretical framework [7, 9, 21–23, 27]. There have also been comparison studies [21, 22, 27] between the SPR approach and the PPR technique, which show that the PPR method works for more types of meshes than the SPR method.

The purpose of this paper is threefold. Firstly, we derive the error estimates for the PDE approach combining the linear FEM. Specifically, we proved the following error estimate for the demagnetizing field:

$$\left\|\vec{\mathrm{H}}_{dem} - \vec{\mathrm{H}}_{dem,h}\right\|_{L^2(\Omega)} \leq Ch\big(\,|\phi_1|_{H^2(\Omega)} + |\phi_2|_{H^2(\Omega)}\,\big) + Ch^{-1/2}\|g - g_h\|_{L^2(\partial\Omega)}, \quad (1.4)$$

where the approximated demagnetizing field $\vec{H}_{dem,h} := -\nabla(\phi_{1,h} + \phi_{2,h})$, $\phi_{i,h}$ is the finite element approximation to ϕ_i $(i = 1, 2)$, g_h is some of the approximation to g. Note that the above error bound consists of two parts: the finite element discretization error and the boundary approximation error. The first part is only of order $\mathcal{O}(h)$ which is one order lower than the error of the best approximation of the demagnetizing field from the finite element space. And it is clear that the lower order convergence of ϕ_1 may also degrade the accuracy of ϕ_2. On the other hand, the boundary approximation calculated on the uniform refined meshes may deteriorate the second part, i.e., the boundary approximation error, due to the singularity in the surface integral. This might

affect the numerical accuracy in the numerical simulation of the Landau-Lifshitz-Gilbert equation.

Secondly, we apply the PPR technique [22] to improve the first part in the above error estimate (1.4). Let G_h be the PPR gradient recovery operator (see Section 3). The following superconvergence result of the PPR approach is established:

$$\left\|\vec{H}_{dem} - (-G_h\phi_h)\right\|_{L^2(\Omega)} \leq C\Big(h^2\left|\phi\right|_{H^3(\Omega)} + h^{1+\rho}\big(\|\phi_1\|_{W^{3,\infty}(\Omega)} + \|\phi_2\|_{W^{3,\infty}(\Omega)}\big) + h^{-1/2}\|g_h - I_h g\|_{L^2(\partial\Omega)}\Big)$$

for some $\rho \in (0, 1]$, see Theorem 3.2. We can see that the convergence order of $\vec{H}_{dem,h}$ can be improved to $\mathcal{O}(h^{1+\rho})$ by using the PPR technique when the boundary value is approximated well. Particularly, the boundary term in the error bound can be removed by taking $g = I_h g$. In contrast, the boundary term of the finite element approximation in (1.4) usually cannot be removed.

Thirdly, we apply a locally refined surface meshes instead of the quasi-uniform surface meshes used in [28] to reduce the error of the approximation for the boundary integral, and hence improve the second part in the error estimate (1.4). The error estimate given above also shows that the approximation of the boundary condition does impact the accuracy of the computation. In order to better approximate the numerical solution, the correction of the boundary condition is needed.

To examine the numerical performance of our method, we code the algorithm using AFEPack [5, 28, 29]. A number of numerical experiments are given to verify the performance of the proposed methods.

This paper is organized as follows. In the next section, the FEM and the error estimate of the finite element solution are shown in detail. In Section 3, the PPR technique with superconvergence properties is described. We also apply the PPR method to improve the accurate calculation. In Section 4, in order to approximate the surface integral in the boundary condition of (1.3), numerical quadratures using locally refined surface meshes are described in depth. In Section 5, a variety of numerical experiments are delivered to show the efficiency of the proposed method. In the last section, the conclusion of the paper is proposed.

2. Finite element method and its error estimates

In this section, we first introduce the finite element discretization of Poisson equations (1.2) and (1.3) and then give the error estimates.

2.1. A brief on the finite element method

We use the linear FEM to solve (1.2) and (1.3). Let $\mathcal{T}_h$ be a regular and quasi-uniform triangulation of Ω and $\mathcal{N}_h$ be the set of all the vertices in the mesh $\mathcal{T}_h$. For any

$T \in \mathcal{T}_h$, let $h_T := \operatorname{diam} T$, and $h := \max h_T$. The finite element space built on $\mathcal{T}_h$ is

$$V_h := \big\{v_h \in C(\bar{\Omega}) : v_h|_T \in P_1(T),\ \forall\, T \subset \mathcal{T}_h\big\},$$

where $P_1(T)$ is the set of polynomials of degree at most 1 on T. We define

$$H^1(\Omega) := \big\{u \in L^2(\Omega) : \partial^\alpha u \in L^2(\Omega) \ \text{ for all } \ |\alpha| \le 1\big\},$$

and the closure of $C_0^\infty(\Omega)$ in $H^1(\Omega)$ is denoted by $H_0^1(\Omega)$.

Introduce a bilinear form $a : H^1(\Omega) \times H^1(\Omega) \to \mathbb{R}$ as

$$a(u, v) = \int_\Omega \nabla u \cdot \nabla v d\vec{x}.$$

Then the variational formulation for (1.2) is to find $\phi_1 \in V := H_0^1(\Omega)$ such that

$$a(\phi_1, v) = (f, v) = \int_\Omega f v dx, \quad \forall v \in V, \tag{2.1}$$

where $f = -\nabla \cdot \vec{\mathrm{M}}(\vec{x})$. Similarly, the variational formulation for the problem (1.3) reads: Find $\phi_2 \in H^1(\Omega)$ and $\phi_2|_{\partial\Omega} = g$ such that

$$a(\phi_2, v) = 0, \quad \forall v \in V. \tag{2.2}$$

The FEM for the problem (1.2) is to find $\phi_{1,h} \in V_h^0 := V_h \cap H_0^1(\Omega)$ such that

$$a(\phi_{1,h}, v_h) = (f, v_h), \quad \forall v_h \in V_h^0. \tag{2.3}$$

And the FEM for the problem (1.3) is to find $\phi_{2,h} \in V_h$ and $\phi_{2,h}|_{\partial\Omega} = g_h$ such that

$$a(\phi_{2,h}, v_h) = 0, \quad \forall v_h \in V_h^0, \tag{2.4}$$

where $g_h \in V_h|_{\partial\Omega}$ is an approximation to g.

Then the finite element approximation of ϕ is given by $\phi_h := \phi_{1,h} + \phi_{2,h}$ and the approximation of the demagnetizing field is given by $\vec{H}_{dem,h} := -\nabla(\phi_{1,h}+\phi_{2,h})$. Noting that the bilinear form $a(\cdot,\cdot)$ is continuous on $H^1(\Omega)\times H^1(\Omega)$ and is coercive on $H_0^1(\Omega)\times H_0^1(\Omega)$. From the Lax-Milgram Lemma [10], we know that both FEMs (2.3) and (2.4) are uniquely solvable. We list three important estimates in FEM, which are needed in the proofs in the Section 2.2. Their proofs and other properties can be found in [10,11].

Lemma 2.1 (Céa Lemma). *Suppose ϕ_i and $\phi_{i,h}$, $i = 1, 2$, are the solutions of the variational problems (*(2.1) *and* (2.2)*) and their Galerkin approximations (*(2.3) *and* (2.4)*), respectively. Then*

$$\|\phi_1 - \phi_{1,h}\|_V \le C \inf_{v_h \in V_h^0} \|\phi_1 - v_h\|_V,$$
$$\|\phi_2 - \phi_{2,h}\|_V \le C \inf_{\substack{v_h \in V_h \\ v_h|_{\partial\Omega} = g_h}} \|\phi_2 - v_h\|_V.$$

From the Céa Lemma, we know that the error of the finite element solution can be bounded by the error of the finite element interpolant. Denote I_h by the standard finite element interpolation operator onto V_h.

Lemma 2.2 (Interpolation Error Estimate)**.** *For $0 \leq i \leq 1$, there exists a positive constant C such that*

$$\|v - I_h v\|_{H^i(\Omega)} \leq Ch^{2-i} |v|_{H^2(\Omega)}, \quad \forall v \in H^2(\Omega).$$

With the quasi-uniform meshes, the following inverse estimate is also useful in the error analysis of the finite element method (see, e.g., [11]).

Lemma 2.3 (Local Inverse Estimate)**.** *For $0 \leq l \leq m$, there exists a constant C such that for all $v_h \in V_h$,*

$$|v_h|_{H^m(T)} \leq Ch^{l-m} |v_h|_{H^l(T)}, \quad \forall T \in \mathcal{T}_h.$$

Lemma 2.4 (Trace Inequality)**.** *Suppose that Ω has a Lipschitz boundary. Then there is a constant C such that*

$$\|v\|_{L^2(\partial\Omega)} \leq C\|v\|^{1/2}_{L^2(\Omega)}\|v\|^{1/2}_{H^1(\Omega)}, \quad \forall v \in H^1(\Omega).$$

2.2. Error estimates

In the following, the error estimations for $\phi_{1,h}$ and $\phi_{2,h}$ will be introduced, respectively. The error estimate of $\phi_{1,h}$ in the following lemma is a direct consequence of the Céa Lemma 1 and the interpolation error estimate Lemma 2.2, whose proof is omitted.

Lemma 2.5. *If the solution $\phi_1 \in H^1_0(\Omega) \cap H^2(\Omega)$, then there exists a constant C independent of h such that*

$$\|\phi_1 - \phi_{1,h}\|_{H^1(\Omega)} \leq Ch |\phi_1|_{H^2(\Omega)}.$$

The next lemma gives the error estimate of $\phi_{2,h}$.

Lemma 2.6. *If the solution $\phi_2 \in H^2(\Omega)$, then there exists a constant C independent of h such that*

$$\|\phi_2 - \phi_{2,h}\|_{H^1(\Omega)} \leq Ch |\phi_2|_{H^2(\Omega)} + Ch^{-1/2}\|g - g_h\|_{L^2(\partial\Omega)}.$$

Proof. Obviously, with Céa Lemma, we have

$$\|\phi_2 - \phi_{2,h}\|_{H^1(\Omega)} \leq C \inf_{\substack{v_h \in V_h \\ v_h|_{\partial\Omega} = g_h}} \|\phi_2 - v_h\|_{H^1(\Omega)}.$$

Let $\mathcal{N}_h$ be the set of all the vertices in the mesh $\mathcal{M}_h$. For any point $z \in \mathcal{N}_h$, let ψ_z be a nodal basis function at z. We set

$$\begin{aligned} v_h &= \sum_{z\in\Omega} \phi_2(z)\psi_z + \sum_{z\in\partial\Omega} g_h(z)\psi_z \\ &= I_h\phi_2 + \sum_{z\in\partial\Omega} \big(g_h(z) - I_h g(z)\big)\psi_z \\ &=: I_h\phi_2 + w_h, \end{aligned} \tag{2.5}$$

where

$$w_h = \sum_{z\in\partial\Omega} \big(g_h(z) - I_h g(z)\big)\psi_z.$$

Clearly, $v_h \in V_h$ and $v_h|_{\partial\Omega} = g_h$. We have,

$$\begin{aligned}\|\phi_2 - \phi_{2,h}\|_{H^1(\Omega)} &\le C\|\phi_2 - I_h\phi_2 - w_h\|_{H^1(\Omega)}\\ &\le C\|\phi_2 - I_h\phi_2\|_{H^1(\Omega)} + C\|w_h\|_{H^1(\Omega)}\\ &\le Ch\,|\phi_2|_{H^2(\Omega)} + C\|w_h\|_{H^1(\Omega)}.\end{aligned}$$

It suffices to analyze $\|w_h\|_{H^1(\Omega)}$. By the inverse estimate Lemma 2.3, we have

$$\begin{aligned}\|w_h\|^2_{H^1(\Omega)} &\le \|w_h\|^2_{L^2(\Omega)} + C\big(h^{-1}\|w_h\|_{L^2(\Omega)}\big)^2\\ &\le Ch^{-2}\|w_h\|^2_{L^2(\Omega)}.\end{aligned}$$

The discussion for the error estimate of last term $\|w_h\|^2_{L^2(\partial\Omega)}$ is given by

$$\begin{aligned}\|w_h\|^2_{L^2(\Omega)} &= \sum_{K\in\mathcal{T}_h}\|w_h\|^2_{L^2(K)} = \sum_{K\in\mathcal{T}_h}\int_K |w_h(x)|^2\,dx\\ &\le \sum_{K\in\mathcal{T}_h}\max_K\big\{w_h^2(x)\big\}\,|K| \le \sum_{K\in\mathcal{T}_h}\max_K\big\{w_h^2(x)\big\}h^3\\ &\le Ch^3\sum_{z\in\mathcal{N}_h} w_h^2(z) = Ch^3\sum_{z\in\mathcal{N}_h\cap\partial\Omega} w_h^2(z)\\ &\le Ch\|w_h\|^2_{L^2(\partial\Omega)}.\end{aligned}$$

Then,

$$\|w_h\|^2_{H^1(\Omega)} \le Ch^{-2}\|w_h\|^2_{L^2(\Omega)} \le Ch^{-1}\|w_h\|^2_{L^2(\partial\Omega)}. \tag{2.6}$$

Obviously, by the triangle inequality, we have

$$\begin{aligned}\|w_h\|_{L^2(\partial\Omega)} &= \|g_h - \phi_2 + \phi_2 - I_h\phi_2\|_{L^2(\partial\Omega)}\\ &\le \|\phi_2 - g_h\|_{L^2(\partial\Omega)} + \|\phi_2 - I_h\phi_2\|_{L^2(\partial\Omega)}.\end{aligned}$$

For $\phi_1|_{\partial\Omega} = 0$, $g|_{\partial\Omega} = \phi_2|_{\partial\Omega}$. And by the Lemmas 2.2 and 2.4, we have

$$\begin{aligned}\|w_h\|_{L^2(\partial\Omega)} &\le \|g - g_h\|_{L^2(\partial\Omega)} + C\|\phi_2 - I_h\phi_2\|^{1/2}_{L^2(\Omega)}\|\phi_2 - I_h\phi_2\|^{1/2}_{H^1(\Omega)}\\ &\le \|g - g_h\|_{L^2(\partial\Omega)} + C\big(Ch^2\,|\phi_2|_{H^2(\Omega)}\big)^{1/2}\big(Ch\,|\phi_2|_{H^2(\Omega)}\big)^{1/2}\\ &\le \|g - g_h\|_{L^2(\partial\Omega)} + Ch^{3/2}\,|\phi_2|_{H^2(\Omega)}.\end{aligned}$$

Finally, the error estimate for ϕ_2 is given by

$$\begin{aligned}\|\phi_2 - \phi_{2,h}\|_{H^1(\Omega)} &\le Ch\,|\phi_2|_{H^2(\Omega)} + Ch^{-1/2}\|w_h\|_{L^2(\partial\Omega)}\\ &\le Ch\,|\phi_2|_{H^2(\Omega)} + Ch^{-1/2}\big(\|g - g_h\|_{L^2(\partial\Omega)} + Ch^{3/2}\,|\phi_2|_{H^2(\Omega)}\big)\\ &\le Ch\,|\phi_2|_{H^2(\Omega)} + Ch^{-1/2}\|g - g_h\|_{L^2(\partial\Omega)} + Ch\,|\phi_2|_{H^2(\Omega)}\\ &\le Ch\,|\phi_2|_{H^2(\Omega)} + Ch^{-1/2}\|g - g_h\|_{L^2(\partial\Omega)}.\end{aligned}$$

This completes the proof of the lemma. □

As a direct consequence of the above two lemmas, we have the following corollary, which gives the H^1 error estimate of ϕ_h.

Corollary 2.1. *Under the conditions of Lemmas* 2.5 *and* 2.6*, we have*

$$\|\phi - \phi_h\|_{H^1(\Omega)} \leq Ch\big(\,|\phi_1|_{H^2(\Omega)} + |\phi_2|_{H^2(\Omega)}\,\big) + Ch^{-1/2}\|g - g_h\|_{L^2(\partial\Omega)}.$$

The following lemma gives the L^2 error estimate of ϕ_h.

Lemma 2.7. *Suppose Ω is convex. Then we have*

$$\|\phi - \phi_h\|_{L^2(\Omega)} \leq Ch^2\big(\,|\phi_1|_{H^2(\Omega)} + |\phi_2|_{H^2(\Omega)}\,\big) + C\|g - g_h\|_{L^2(\partial\Omega)}.$$

Proof. This lemma can be proved by the duality argument, Lemmas 2.5 and 2.6. Here, we use duality argument to approximate the difference $\phi - \phi_h$ in L^2 norm. Let $u \in H_0^1(\Omega)$ be the solution of the problem

$$-\Delta u = \phi - \phi_h \quad \text{in } \Omega.$$

Then the variational formulation of this problem is to find $u \in H_0^1(\Omega)$ such that

$$a(u, v) = (\phi - \phi_h, v), \quad \forall v \in H_0^1(\Omega).$$

It is clear that the above problem attains a unique solution, hence

$$\begin{aligned}
\|\phi - \phi_h\|_{L^2(\Omega)}^2 &= (\phi - \phi_h, \phi - \phi_h) = (\phi - \phi_h, -\Delta u) \\
&= a(\phi - \phi_h, u) - \int_{\partial\Omega} \nabla u \cdot \vec{n}(\phi - \phi_h) \\
&= a(\phi - \phi_h, u - I_h u) - \int_{\partial\Omega} \nabla u \cdot \vec{n}(g - g_h) \\
&\leq C\|\phi - \phi_h\|_{H^1(\Omega)}\|u - I_h u\|_{H^1(\Omega)} + \|\nabla u\|_{L^2(\partial\Omega)}\|g - g_h\|_{L^2(\partial\Omega)} \\
&\leq Ch\|\phi - \phi_h\|_{H^1(\Omega)}\,|u|_{H^2(\Omega)} + C\|u\|_{H^2(\Omega)}\|g - g_h\|_{L^2(\partial\Omega)},
\end{aligned}$$

where we used Lemma 2.4 to derive the last inequality. Since there holds the regularity estimate $\|u\|_{H^2(\Omega)} \leq C\|\phi - \phi_h\|_{L^2(\Omega)}$, then we have

$$\begin{aligned}
\|\phi - \phi_h\|_{L^2(\Omega)} &\leq Ch\|\phi - \phi_h\|_{H^1(\Omega)} + C\|g - g_h\|_{L^2(\partial\Omega)} \\
&\leq Ch\big(h(|\phi_1|_{H^2(\Omega)} + |\phi_2|_{H^2(\Omega)}) + h^{-1/2}\|g - g_h\|_{L^2(\partial\Omega)}\big) \\
&\quad + C\|g - g_h\|_{L^2(\partial\Omega)} \\
&\leq Ch^2\big(\,|\phi_1|_{H^2(\Omega)} + |\phi_2|_{H^2(\Omega)}\,\big) + C\|g - g_h\|_{L^2(\partial\Omega)}.
\end{aligned}$$

This completes the proof of the lemma. □

Remark 2.1. When the domain has re-entrant corners, locally refined meshes of Ω together with the adaptive technique [20] will be more efficient, which will be considered in a future work.

As a consequence of Lemma 2.7, we have the following theorem which gives the error estimates of the demagnetizing field approximation and the discrete energy.

Theorem 2.1. *Suppose $\phi_i \in H^2(\Omega)$, $i = 1, 2$. Then we have*

$$\|\vec{\mathrm{H}}_{dem} - \vec{\mathrm{H}}_{dem,h}\|_{L^2(\Omega)} \le Ch\big(\,|\phi_1|_{H^2(\Omega)} + |\phi_2|_{H^2(\Omega)}\,\big) + Ch^{-1/2}\|g - g_h\|_{L^2(\partial\Omega)},$$
$$|E_{dem} - E_{dem,h}| \le Ch\big(\,|\phi_1|_{H^2(\Omega)} + |\phi_2|_{H^2(\Omega)}\,\big) + Ch^{-1/2}\|g - g_h\|_{L^2(\partial\Omega)}.$$

Proof. It is easy to get the proof for the first part,

$$\begin{aligned}\|\vec{\mathrm{H}}_{dem} - \vec{\mathrm{H}}_{dem,h}\|_{L^2(\Omega)} &= \|\nabla\phi - \nabla\phi_h\|_{L^2(\Omega)} \le \|\phi - \phi_h\|_{H^1(\Omega)}\\ &\le \|\phi_1 - \phi_{1,h}\|_{H^1(\Omega)} + \|\phi_2 - \phi_{2,h}\|_{H^1(\Omega)}\\ &\le Ch\big(\,|\phi_1|_{H^2(\Omega)} + |\phi_2|_{H^2(\Omega)}\,\big) + Ch^{-1/2}\|g - g_h\|_{L^2(\partial\Omega)}.\end{aligned}$$

Then, by the definition of the demagnetizing field energy and Holder inequality, we have

$$\begin{aligned}|E_{dem} - E_{dem,h}| &= \left|-\frac{\mu_0}{2}\int_\Omega \big(\vec{\mathrm{H}}_{dem} - \vec{\mathrm{H}}_{dem,h}\big)\cdot\vec{\mathrm{M}}dx\right|\\ &\le \frac{\mu_0}{2}\big\|\vec{\mathrm{H}}_{dem} - \vec{\mathrm{H}}_{dem,h}\big\|_{L^2(\Omega)}\cdot\|\vec{\mathrm{M}}\|_{L^2(\Omega)}\\ &\le C\big\|\vec{\mathrm{H}}_{dem} - \vec{\mathrm{H}}_{dem,h}\big\|_{L^2(\Omega)},\end{aligned}$$

then, obviously, we can get the proof. □

Note that the above error bound consists of two parts, i.e., the finite element discretization error and the boundary approximation error. The first part is only of order $\mathcal{O}(h)$, which is one order lower than the error of the best approximation of the demagnetizing field from the finite element space. To improve the finite element discretization error, in Section 3, we apply the PPR technique [22] to recover the gradient of the numerical solution. On the other hand, the boundary approximation calculated on the uniform refined meshes may deteriorate the second part, i.e., the boundary approximation error, due to the singularity in the surface integral. To solve this issue, in Section 4, we apply locally refined surface meshes to compute the boundary integral.

3. The PPR gradient recovery

In this section, we apply the PPR technique to improve the finite discretization error of $\nabla\phi_h$, and hence improve the first part the error bound of the discrete demagnetizing field. The superconvergence of the PPR technique has also been developed, based on the result in [8].

3.1. PPR formulation

In this part, the PPR technique is defined under the following simple observations: The basis functions of V_h are the nodal basis functions. Therefore, each function in V_h is uniquely defined by its values at the mesh nodes. Let $\{v_s : s \in \mathcal{N}_h\}$ be the Lagrange basis of V_h, and let $G_h\phi_h \in V_h \times V_h$ denote the gradient recovery operator.

We begin with the definition of the PPR-recovered gradient $G_h\phi_h$ at a node $s \in \mathcal{N}_h$ by the following three steps, where $G_h : C(\Omega) \mapsto V_h \times V_h$. Roughly speaking, first we select $n \geq 10$ sampling nodes $s_1 = s, s_2, \cdots, s_n$ in an element patch ω_s. Then, find a quadratic polynomial $p \in P_2(\omega_s)$ which best fits ϕ_h at those sampling nodes, in the least squares sense. Here $P_2(\omega_s)$ denotes the space of quadratic polynomials defined on ω_s. Finally, the recovered gradient at s is given by

$$G_h\phi_h(s) = (\nabla p)(s).$$

Furthermore, the PPR-recovered gradient $G_h\phi_h$ has the following properties [13, 23]:

1. By definition, G_h is linear.
2. G_h satisfies the consistency condition, i.e., $G_h(I_h p) = \nabla p,\ \forall p \in P_2(\Omega)$.
3. G_h satisfies the approximation property, i.e.,

$$\|\nabla u - G_h(I_h u)\|_{L^2(\Omega)} \leq Ch^2 \left|u\right|_{H^3(\Omega)}, \quad \forall u \in H^3(\Omega). \tag{3.1}$$

4. G_h is bounded, i.e.,

$$\|G_h u\|_{L^2(\Omega)} \leq C \left|u\right|_{H^1(\Omega)}. \tag{3.2}$$

In implementation, the sampling nodes can be first selected from s and its immediately neighboring nodes (i.e., the nodes directly attached with s, see, e.g., Fig. 1(a)). If the number of them is less than 10, then we can select more sampling nodes from the immediately neighboring nodes of some of the immediately neighboring nodes of s, and so on, until the number of the sampling nodes $n \geq 10$ (see, e.g., Fig. 1(b)).

Regard to the gradient recovery of the ϕ_h with the PPR technique, we would find the quadratic polynomial p best fits ϕ_h, which is to find $p \in P_2(\omega_s)$ such that

$$\sum_{j=1}^{n}(p - \phi_h)^2(s_j) = \min_{p \in P_2}\sum_{j=1}^{n}(p - \phi_h)^2(s_j).$$

Denote by (x_i, y_i, z_i) the coordinates of the node s_i. To reduce the round-off error, we introduce a constant h_s which denotes the maximum distance between the sampling node s_i $(i = 2, \ldots, n)$ and the node $s = s_1$, and write the quadratic polynomial p as

$$p = a_0 + a_1\left(\frac{x - x_1}{h_s}\right) + a_2\left(\frac{y - y_1}{h_s}\right) + a_3\left(\frac{z - z_1}{h_s}\right) + a_4\left(\frac{x - x_1}{h_s}\right)^2$$

$$+a_5\left(\frac{y-y_1}{h_s}\right)^2+a_6\left(\frac{z-z_1}{h_s}\right)^2+a_7\left(\frac{x-x_1}{h_s}\right)\left(\frac{y-y_1}{h_s}\right)$$
$$+a_8\left(\frac{x-x_1}{h_s}\right)\left(\frac{z-z_1}{h_s}\right)+a_9\left(\frac{y-y_1}{h_s}\right)\left(\frac{z-z_1}{h_s}\right).$$

Let

$$\mathbf{a}=\begin{bmatrix}a_0 & a_1 & a_3 & a_4 & a_5 & a_6 & a_7 & a_8 & a_9\end{bmatrix}^T,$$
$$\xi_i=\frac{x_i-x_0}{h},\quad \eta_i=\frac{y_i-y_0}{h},\quad \gamma_i=\frac{z_i-z_0}{h},$$

and

$$A=\begin{bmatrix}1 & \xi_1 & \eta_1 & \gamma_1 & \xi_1^2 & \eta_1^2 & \gamma_1^2 & \xi_1\eta_1 & \xi_1\gamma_1 & \eta_1\gamma_1\\ 1 & \xi_2 & \eta_2 & \gamma_2 & \xi_2^2 & \eta_2^2 & \gamma_2^2 & \xi_2\eta_2 & \xi_2\gamma_2 & \eta_2\gamma_2\\ \vdots & \vdots & \vdots & \vdots & \vdots & \vdots & \vdots & \vdots & \vdots & \vdots\\ 1 & \xi_n & \eta_n & \gamma_n & \xi_n^2 & \eta_n^2 & \gamma_n^2 & \xi_n\eta_n & \xi_n\gamma_n & \eta_n\gamma_n\end{bmatrix}_{n\times 10},\quad \Phi_h=\begin{bmatrix}\phi_h(s_1)\\ \phi_h(s_2)\\ \vdots\\ \phi_h(s_n)\end{bmatrix}_{n\times 1}.$$

It is easy to find that

$$\mathbf{a}=(A^TA)^{-1}A^T\Phi_h, \tag{3.3}$$

and the recovered gradient at s

$$G_h\phi_h(s)=\begin{bmatrix}\partial_x p(s) & \partial_y p(s) & \partial_z p(s)\end{bmatrix}^T=\frac{1}{h}\begin{bmatrix}a_1 & a_2 & a_3\end{bmatrix}^T.$$

If $\det(A^TA)=0$ or is excessively small, for instance, $|\det(A^TA)|<10^{-8}$, the existence or stability of the least square solution may not be guaranteed. In such a case, it is necessary to incorporate additional sampling nodes, selected from the neighboring nodes of the existent sampling nodes as described above, and then solve the Eq. (3.3) with the updated group of sampling nodes.

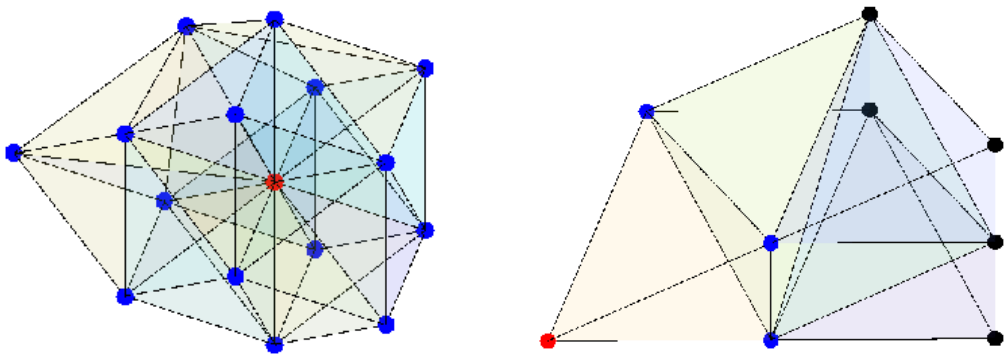

(a) (b)

Figure 1: Sampling nodes in PPR: The red node represents the target node s, the blue nodes correspond to the immediately neighboring nodes of s, and the black nodes indicate the immediately neighboring nodes of two immediately neighboring nodes of s. (a) s has at least 9 immediately neighboring nodes; (b) s has fewer than 9 immediately neighboring nodes.

3.2. Superconvergence estimates

In general, a point-symmetric domain for the triangulation $\mathcal{T}_h$ is not frequently formed by two adjacent tetrahedra sharing a face. For the 3-dimensional case, based on the tips for the PPR and the framework in [8, 9, 23], the following constraint is required for the triangulation in order to achieve the superconvergence performance for 3D problems.

Definition 3.1 ([8]). *In the 3-dimensional space, the triangulation $\mathcal{T}_h = \mathcal{T}_{1,h} \cup \mathcal{T}_{2,h}$ is said to satisfy the condition (α, σ) if there exist positive constants α and σ such that the lengths of each pair of opposite edges in each 3-face of every 3-simplex inside $\mathcal{T}_{1,h}$ differ only by $\mathcal{O}(h^{1+\alpha})$ and*

$$\bar{\Omega}_{1,h} \cup \bar{\Omega}_{2,h} = \bar{\Omega}, \quad |\Omega_{2,h}| = \mathcal{O}(h^{\sigma}), \quad \bar{\Omega}_{i,h} = \bigcup_{\tau \in \mathcal{T}_{i,h}} \bar{\tau}, \quad i = 1, 2.$$

Since it is the tetrahedron and belongs to the good region, then the edge lengths must satisfy the following condition:

$$\max\left\{ |d_{kl} - d_{mo}|, |d_{km} - d_{lo}|, |d_{ko} - d_{lm}| \right\} \lesssim h^{1+\alpha},$$

where d_{ij} denotes the edge length between s^i and s^j. If $(\alpha, \sigma) = (\infty, \infty)$, the mesh is said to satisfy the exact edge pair condition, i.e., each pair of opposite edges in each 3-face of a 3-simplex has the same length.

Then two neighboring tetrahedrons are essentially similar and do not have incredibly tiny angles because of the constraints mentioned above on the mesh. The superconvergence estimate between the finite element approximation and the interpolant of ϕ_1 is given in the following lemma, due to [8, Theorem 3.6].

Lemma 3.1 ([8]). *Let the solution $\phi_1 \in W^{3,\infty}(\Omega)$. Assume that the tetrahedralization $\mathcal{T}_h$ satisfies the edge pair condition with parameters (α, σ). Then*

$$\|\phi_{1,h} - I_h\phi_1\|_{H^1(\Omega)} \leq Ch^{1+\rho}\|\phi_1\|_{W^{3,\infty}(\Omega)}, \quad \rho = \min\left(\alpha, \frac{\sigma}{2}, 1\right),$$

where C is a constant.

Similar to the above lemma, the superconvergence estimate between $\phi_{2,h}$ and $I_h\phi_2$ is given in the following theorem.

Theorem 3.1 ([8]). *Let the solution $\phi_2 \in W^{3,\infty}(\Omega)$. Assume that the tetrahedralization $\mathcal{T}_h$ satisfies the edge pair condition with parameters (α, σ). Then*

$$\|\phi_{2,h} - I_h\phi_2\|_{H^1(\Omega)} \leq Ch^{1+\rho}\|\phi_2\|_{W^{3,\infty}(\Omega)} + Ch^{-1/2}\|g_h - I_h g\|_{L^2(\partial\Omega)}, \quad \rho = \min\left(\alpha, \frac{\sigma}{2}, 1\right).$$

Proof. First we consider

$$\begin{aligned}
&\|\phi_{2,h} - I_h\phi_2 - w_h\|_{H^1(\Omega)} \\
&\le C \sup_{v_h \in V_h^0} \frac{a(\phi_{2,h} - I_h\phi_2 - w_h, v_h)}{\|v_h\|_{H^1(\Omega)}} \\
&\le C \sup_{v_h \in V_h^0} \frac{a(\phi_2 - I_h\phi_2 - w_h, v_h)}{\|v_h\|_{H^1(\Omega)}} \\
&\le C \sup_{v_h \in V_h^0} \left(\frac{a(\phi_2 - I_h\phi_2, v_h)}{\|v_h\|_{H^1(\Omega)}} + \frac{a(w_h, v_h)}{\|v_h\|_{H^1(\Omega)}} \right) \\
&\le C\big(h^{1+\rho}\|\phi_2\|_{W^{3,\infty}(\Omega)} + \|w_h\|_{H^1(\Omega)}\big),
\end{aligned}$$

where the definition of w_h is given in (2.5). From the estimate (2.6), we obtain

$$\|\phi_{2,h} - I_h\phi_2 - w_h\|_{H^1(\Omega)} \le C\big(h^{1+\rho}\|\phi_2\|_{W^{3,\infty}(\Omega)} + h^{-1/2}\|w_h\|_{L^2(\partial\Omega)}\big).$$

Obviously, we have

$$\begin{aligned}
\|\phi_{2,h} - I_h\phi_2\|_{H^1(\Omega)} &\le \|\phi_{2,h} - I_h\phi_2 - w_h\|_{H^1(\Omega)} + \|w_h\|_{H^1(\Omega)} \\
&\le C\big(h^{1+\rho}\|\phi_2\|_{W^{3,\infty}(\Omega)} + h^{-1/2}\|w_h\|_{L^2(\partial\Omega)}\big) \\
&\le C\big(h^{1+\rho}\|\phi_2\|_{W^{3,\infty}(\Omega)} + h^{-1/2}\|g_h - I_h g\|_{L^2(\partial\Omega)}\big).
\end{aligned}$$

The proof is complete. □

With the interpolation error estimates we have gotten, the superconvergence property of the PPR technique for ϕ can be given in the following theorem.

Theorem 3.2. *The polynomial preserving recovery $G_h\phi_h$ satisfies the following estimation:*

$$\begin{aligned}
\big\|\vec{H}_{dem} - (-G_h\phi_h)\big\|_{L^2(\Omega)} \le C\Big(&h^2\,|\phi|_{H^3(\Omega)} + h^{1+\rho}(\|\phi_1\|_{W^{3,\infty}(\Omega)} + \|\phi_2\|_{W^{3,\infty}(\Omega)}) \\
&+ h^{-1/2}\|g_h - I_h g\|_{L^2(\partial\Omega)}\Big),
\end{aligned}$$

where $\rho = \min(\alpha, \sigma/2, 1)$.

Proof. Obviously,

$$\begin{aligned}
&\big\|\vec{H}_{dem} - (-G_h\phi_h)\big\|_{L^2(\Omega)} \\
&= \|\nabla\phi - G_h(I_h\phi) + G_h(I_h\phi) - G_h\phi_h\|_{L^2(\Omega)} \\
&\le \|\nabla\phi - G_h(I_h\phi)\|_{L^2(\Omega)} + \|G_h(I_h\phi) - G_h\phi_h\|_{L^2(\Omega)}.
\end{aligned}$$

The first term can be easily estimated by using (3.1), so that

$$\|\nabla\phi - G_h(I_h\phi)\|_{L^2(\Omega)} \le Ch^2\,|\phi|_{H^3(\Omega)}\,.$$

For the second term, it is easy to get that

$$G_h(I_h\phi) - G_h\phi_h = G_h(I_h\phi - \phi_h),$$

and with the boundedness of G_h, see (3.2), we have

$$\begin{aligned} &\|G_h(I_h\phi) - G_h\phi_h\|_{L^2(\Omega)} \\ \le\ &\|\nabla(I_h\phi - \phi_h)\|_{L^2(\Omega)} \\ \le\ &\|I_h\phi_1 - \phi_{1,h}\|_{H^1(\Omega)} + \|I_h\phi_2 - \phi_{2,h}\|_{H^1(\Omega)}. \end{aligned}$$

Then, by Lemma 3.1 and Theorem 3.1, we have

$$\begin{aligned} \|\nabla\phi - G_h\phi_h\|_{L^2(\Omega)} \le C\Big(&h^2\,|\phi|_{H^3(\Omega)} + h^{1+\rho}(\|\phi_1\|_{W^{3,\infty}(\Omega)} + \|\phi_2\|_{W^{3,\infty}(\Omega)}) \\ &+ h^{-1/2}\|g_h - I_h g\|_{L^2(\partial\Omega)}\Big), \end{aligned}$$

where $\rho = \min(\alpha, \sigma/2, 1)$. This completes the proof. □

Remark 3.1. From Theorem 3.2, we know that the convergence order of $\vec{H}_{dem,h}$ can be improved to $\mathcal{O}(h^{1+\rho})$ by using the PPR technique when the boundary value is approximated well. Particularly, the boundary term in the error bound can be removed by taking $g = I_h g$. By contrast, the boundary term of the finite element approximation in Theorem 2.1 usually cannot be removed.

4. Reconstruction for surface meshes

In order to guarantee the superconvergence property of the PPR recovery in Theorem 3.2 in numerical simulations, it is necessary to accurately calculate the singular boundary integral in (1.3). For simplicity, we write g at a point $\vec{x}_0 \in \partial\Omega$ as

$$g(\vec{x}_0) = \int_{\partial\Omega} F(\vec{x}_0, \vec{x})d\vec{x}, \quad F := N(\vec{x}_0 - \vec{x})\left(\vec{\mathrm{M}}(\vec{x}) \cdot \vec{n}(\vec{x}) + \frac{\partial\phi_1}{\partial\vec{n}}(\vec{x})\right). \tag{4.1}$$

Clearly, F is singular at $\vec{x}_0$. Although the triangulation $\mathcal{T}_h$ of Ω induces a surface mesh of the boundary $\partial\Omega$, it is quasi-uniform and not suitable for computing the above singular integral. This motivated us to reconstruct a locally refined surface mesh to improve the calculations on the boundary. However, it is not easy to reconstruct a proper locally refined mesh on the surface of a general domain. For simplicity, we only show the idea of reconstruction in detail and present quadrature formula for approximating (4.1) for two cases, i.e., a unit sphere and the surface of a unit cube, respectively, in the following subsections.

4.1. A unit sphere case

Firstly, we introduce an approach to improve the numerical integral on the boundary $\partial\Omega$ of a sphere. For simplicity, we use the unit sphere as an example. Obviously, it is more convenient to compute the integral on the sphere by using the spherical coordinate system. For a given node (r,θ,ϕ) in spherical coordinates, its Cartesian coordinates (x,y,z) is given by

$$x = r\sin\theta\cos\varphi, \quad y = r\cos\theta\sin\varphi, \quad z = r\cos\theta,$$

where r is the radius of the sphere, $0 \le \theta \le 2\pi$ is the angle from the x-axis to the line between the projection of the node on the xy-plane and the origin, and $0 \le \varphi \le \pi$ denotes the angle from the line between the node and the origin to the positive z-axis.

First, for simplicity, we suppose that the singular node is located at the North Pole, and construct a mesh which is locally refined at the node $(0,0,1)$ (in Cartesian coordinates). Given a positive integer n, let $\theta_i = i\pi/n$ and $\varphi_j = j\pi/n$. We introduce the following partition of the unit sphere:

$$\mathcal{T} := \big\{K_{ij} : K_{ij} = \{(r,\theta,\phi) :\ r = 1,\ \theta_{i-1} \le \theta \le \theta_i,\ \phi_{j-1} \le \phi \le \phi_j\},\\ i = 1,\dots,2n,\ j = 1,\dots,n\big\}.$$

Although the partition is uniform in spherical coordinates with respect to θ and φ, it is locally refined in Cartesian coordinates at the pole (see Fig. 2).

Then, for the general case, suppose the singular node is located at $\vec{x}_0$ with Cartesian coordinate (x_0,y_0,z_0) and spherical coordinate $(1,\theta_0,\varphi_0)$. We just need to use a rotation transformation to rotate the North Pole to $\vec{x}_0$ and use the above mesh instead of having to construct a new mesh. This can be done by using the Rodrigues' rotation formula as follows.

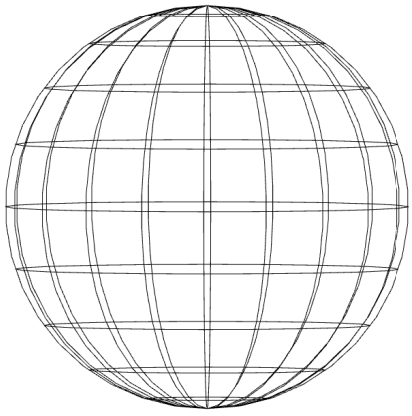

Figure 2: The construction for the unit sphere ($n = 10$ as an example).

We choose the axis of rotation to be the following unit vector on the xy-plane, which is perpendicular to (x_0, y_0, z_0):

$$\omega = \begin{bmatrix} \omega_x \\ \omega_y \\ \omega_z \end{bmatrix} = \frac{1}{\sqrt{x_0^2 + y_0^2}} \begin{bmatrix} y_0 \\ -x_0 \\ 0 \end{bmatrix}.$$

It is clear that the North Pole can be rotated to the node $\vec{x}_0$ by rotating the unit sphere by the angle $-\varphi_0$ around the axis ω. Meanwhile, by Rodrigues' rotation formula, any node $\vec{x} = (x, y, z)^T$ on the sphere can be rotated to the node $\hat{\vec{x}} = (\hat{x}, \hat{y}, \hat{z})^T$

$$\begin{bmatrix} \hat{x} \\ \hat{y} \\ \hat{z} \end{bmatrix} = R(-\varphi_0) \begin{bmatrix} x \\ y \\ z \end{bmatrix},$$

where the rotation matrix

$$R(\theta) = \begin{bmatrix} R1 & R2 & R3 \end{bmatrix}$$

and

$$R1 = \begin{bmatrix} \cos\theta + \omega_x^2(1-\cos\theta) \\ \omega_x\omega_y(1-\cos\theta) + \omega_z\sin\theta \\ \omega_x\omega_z(1-\cos\theta) - \omega_y\sin\theta) \end{bmatrix},$$
$$R2 = \begin{bmatrix} \omega_x\omega_y(1-\cos\theta) - \omega_x\sin\theta \\ \cos\theta + \omega_y^2(1-\cos\theta) \\ \omega_y\omega_z(1-\cos\theta) + \omega_x\sin\theta) \end{bmatrix},$$
$$R3 = \begin{bmatrix} \omega_x\omega_z(1-\cos\theta) + \omega_y\sin\theta \\ \omega_y\omega_z(1-\cos\theta) - \omega_x\sin\theta \\ \cos\theta + \omega_z^2(1-\cos\theta) \end{bmatrix}.$$

Next, we calculate the integral in (4.1). Let $\Delta\theta = \Delta\varphi = \pi/n := h$. Each element K_{ij} is a curvilinear trapezoid, we take its centroid point $\vec{x}_{ij} : (r, \theta_{ij}, \varphi_{ij})$ as the integral node, where $\theta_{ij} = (\theta_{i-1} + \theta_i)/2$ and $\varphi_{ij} = (\varphi_{j-1} + \varphi_j)/2$. The height of $K_{ij} \approx r\Delta\varphi$, and its two bases $\approx r\Delta\theta\sin(\varphi_{ij} \pm \Delta\varphi/2)$. So the area of this element can by approximated by

$$\begin{aligned} |K_{ij}| &\approx \frac{1}{2}(r\Delta\varphi)\left(r\Delta\theta\sin\left(\varphi_{ij} - \frac{\Delta\varphi}{2}\right) + r\Delta\theta\sin\left(\varphi_{ij} + \frac{\Delta\varphi}{2}\right)\right) \\ &= r^2\sin\varphi_{ij}\cos\frac{\Delta\varphi}{2}\Delta\theta\Delta\varphi \\ &\approx r^2\sin\varphi_{ij}\Delta\theta\Delta\varphi. \end{aligned}$$

Then the integral in (4.1)

$$\begin{aligned} g(\vec{x_0}) &= \int_{\partial\Omega} F(\vec{x}_0, \hat{\vec{x}}) d\hat{\vec{x}} = \int_{\partial\Omega} F(\vec{x}_0, \hat{\vec{x}}) d\vec{x} \\ &= \sum_{K_{ij}\in\mathcal{T}} \int_{K_{ij}} F(\vec{x}_0, \hat{\vec{x}}) d\vec{x} \approx \sum_{K_{ij}\in\mathcal{T}} F(\vec{x}_0, \hat{\vec{x}}_{ij}) \, |K_{ij}| \\ &= \sum_{K_{ij}\in\mathcal{T}} F(\vec{x}_0, \hat{\vec{x}}_{ij}) r^2 \sin\varphi_{ij} \Delta\theta\Delta\varphi \\ &= \sum_{K_{ij}\in\mathcal{T}} F(\vec{x}_0, \hat{\vec{x}}_{ij}) r^2 \sin\varphi_{ij} h^2 =: g_h(\vec{x}_0). \end{aligned}$$

Finally, we demonstrate the convergence order of the corrected approximation g_h by a numerical example from Section 5.1. Fig. 3 shows that the convergence order for the original approximation using a quasi-uniform surface mesh is about $\mathcal{O}(h)$ in L^2-norm, while the convergence order of the corrected approximation using the above locally refined mesh is about $\mathcal{O}(h^2)$.

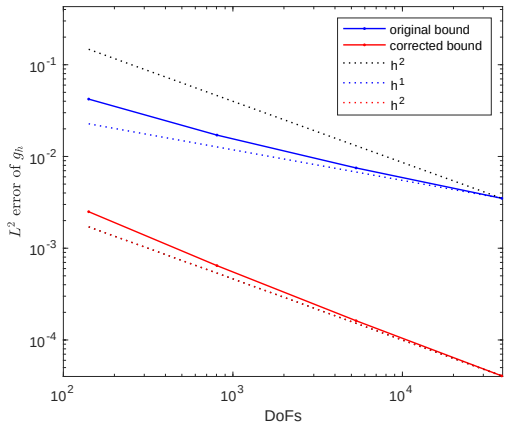

Figure 3: L^2 error of g_h.

4.2. A unit cube case

Spherical coordinates are not appropriate anymore for the cube case. In this subsection, we focus on the Cartesian coordinate system. Here, we introduce the way to reconstruct the boundary integral, in which a unit cube is chosen as an example.

The notations for the faces of the unit cube are shown in Fig. 4(a). Suppose that the singular integral node $s_0 : (x_0, y_0, z_0)$ is on the bottom of the cube ($z_0 = -0.5$), but not on any edge of the cube. In order to resolve the singularity at s_0, we construct a locally refined mesh as follows.

We first divide the bottom of the cube into four triangles $(\triangle A, \triangle B, \triangle C, \triangle D)$, by connecting s_0 to the 4 vertices of the bottom, as shown in Fig. 4(b).

Then we construct a locally refined mesh for each triangle, taking the $\triangle A$ as an example, which is shown in Fig. 4(b). The construction will be done in two steps. First, we divide the base of $\triangle A$ into $n = 2m$ parts equally with nodes $\{s_j : (0.5, y_j, -0.5)\}_{j=1}^{n+1}$, where $y_j = -0.5 + (j-1)h$ and $h = 1/n$, and connect the node s_0 with each s_j. Then, divide the triangle equally into m parts in the other direction by drawing $m-1$ lines parallel to the base

$$x = x_i := x_0 + 2ih(0.5 - x_0), \quad z = -0.5,$$

where $i = 1, \ldots, m$. Therefore, the triangle has been divided into mn elements, which is shown in Fig. 4(b). Denote K_{ij} as the element in the i-th volume and the j-th row, that is the quadrilateral surrounded by four lines: $x = x_{i-1}$, $x = x_i$, $\overline{s_0 s_j}$, $\overline{s_0 s_{j+1}}$. By simple calculations, we find that the area of K_{ij} is $|K_{ij}| = 2h^3(2i-1)$ and the center point of K_{ij} is $\vec{v_{ij}} : (x_{ij}, y_{ij}, z_{ij})$, where

$$x_{ij} := \frac{x_{i-1} + x_i}{2}, \quad y_{ij} := y_0 + h(2i-1)\left(-0.5 + jh - y_0 - \frac{h}{2}\right), \quad z_{ij} := -0.5.$$

Then the integral in (4.1) on $\triangle A$ is

$$\int_{\triangle A} F(\vec{x_0}, \vec{x}) d\vec{x} = \sum_{i=1}^{m}\sum_{j=1}^{n} \int_{K_{ij}} F(\vec{x_0}, \vec{x}) d\vec{x} \approx \sum_{i=1}^{m}\sum_{j=1}^{n} F(\vec{x_0}, \vec{v_{ij}}) \, |K_{ij}| \, . \tag{4.2}$$

This construction is also applied to the other three triangles. The partition for the bottom has been finished.

Since the top face is faraway from the singular node s_0, we just use a uniform partition to separate it into n^2 small squares.

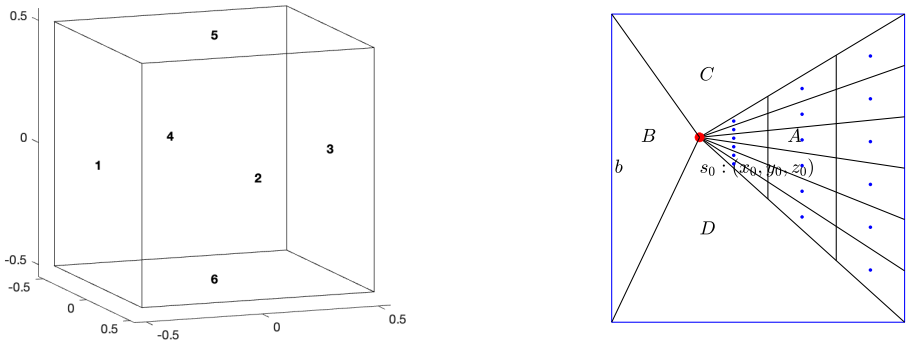

(a) (b)

Figure 4: (a): notation for each face of the unit cube, (b): the approach to separate the Face 6 (the bottom one) into 4 parts and the partition for Part A, $n = 2m = 6$ as an example.

Next, we consider the partition for the other faces. We take Face 4 (see Fig. 5) as an example, which shares the same edge b of the bottom. Because the singular node s_0 may close to the edge b, we construct a locally refined mesh for this face as follows.

Let s_0' be the foot of s_0 perpendicular to the edge b. Then we split the face into three triangles by connecting the vertices on the opposite edge of b with s_0', as shown in Fig. 5. Then we construct a locally refined mesh for these three triangles in the same way that we have done to $\triangle A$. The integral on each triangle can be approximated in a similar way to (4.2). We omit the details.

If the singular node is situated on a face other than the bottom one, a rotation transformation can be applied to move the singular node to the bottom face, allowing the integral to be calculated as described above. The validation of the proposed method in this subsection will be done in next section.

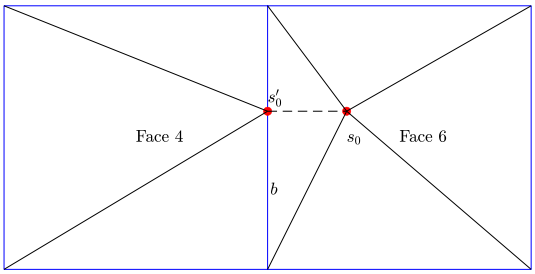

Figure 5: The partition for proximal faces of the bottom.

5. Numerical experiments

To numerically check the proposed methods in previous sections, three numerical experiments will be done in this section. We first solve a model problem with a homogeneous magnetization in a unit sphere, where the exact solutions to both the demagnetizing field and its energy are known. The second problem is the case with homogeneous magnetization on a unit cube, whose demagnetizing field energy is known. The last problem is a vortex state of the magnetization field on a unit cube. For the last problem, we use the approximate solution on the mesh with 1 million degrees of freedom as the reference result.

We will, from the following aspects, show the effectiveness of the proposed methods, i.e., i) the recovered gradient from our method is superior to the one from SPR, which confirms results from [22], implying that the proposed method and the code work well, and ii) the correction introduced in Subsection 4 works well for delivering the desired convergence of the demagnetizing field, and iii) the superconvergence order of the demagnetizing field using our proposed PDE approach can be obtained smoothly.

It is noted that the code is developed based on AFEMAG [5,28,29], and all numerical simulations are implemented using a MacBook Pro with an Apple M2 Pro CPU, and 16 gigabytes memory.

5.1. The homogeneous magnetization field in a unit sphere

The homogeneous magnetization in this part is $\vec{\mathrm{M}} = (0, 0, 1)$. The computational domain is a unit sphere with center point at $(0, 0, 0)$. It is known that the demagnetizing field factor for this problem is $4\pi/3$. Hence, the demagnetizing field for this example is also a homogeneous one with $\vec{\mathrm{H}}_{dem} = -\vec{\mathrm{M}}/3$ and the analytical demagnetizing field energy is $2\pi/9$.

The following table demonstrates a comparison of the errors for the demagnetizing field energy from the SPR and the PPR, respectively. From Table 1, it is observed that both the error and the convergence from two methods are very similar, which can be explained by the good configuration of the problem. It can also be observed that the convergence order becomes first order with the increment of mesh grids, which can be explained by the inaccurate calculation of the boundary conditions in the PDE approach, according to Theorem 2.1 in Subsection 2.2.

We have proved that the method which has been shown in Subsection 4.1 is to reconstruct the surface meshes improved the accurate calculation of the boundary integral in this example. Then we turn to the calculation for the demagnetizing field energy with different methods, and the results are shown below.

To show the efficiency of the method for the correction of the boundary, the performances for the convergence properties of different methods are shown in Fig. 6. Three conclusions will be bravely given from the results. First, we can obviously find out that the results of the demagnetizing field energy are the same under both the SPR and the PPR techniques in Fig. 6(a), for the problem is a linear element problem and the solution given by the finite element method is good enough. Second, in Fig. 6(b), the error convergence orders achieved using the techniques with corrected boundary integrals exceed second-order and exhibit a trend toward second-order superconvergence. Finally, the results with the corrected boundary integral are better than those with the original boundary integral under both the SPR and the PPR techniques.

Table 1: The numerical results for the problem in this subsection. The error and the order for computing the E_{dem} by SPR and PPR techniques on a unit sphere.

Mesh(Dofs)	err_{SPR}	Order	err_{PPR}	Order
Ball0(141)	0.07588		0.11745	
Ball1(805)	0.02590	1.8512	0.02759	2.4949
Ball2(5329)	0.00976	1.5492	0.00970	1.6594
Ball3(38529)	0.00407	1.3256	0.00410	1.3047

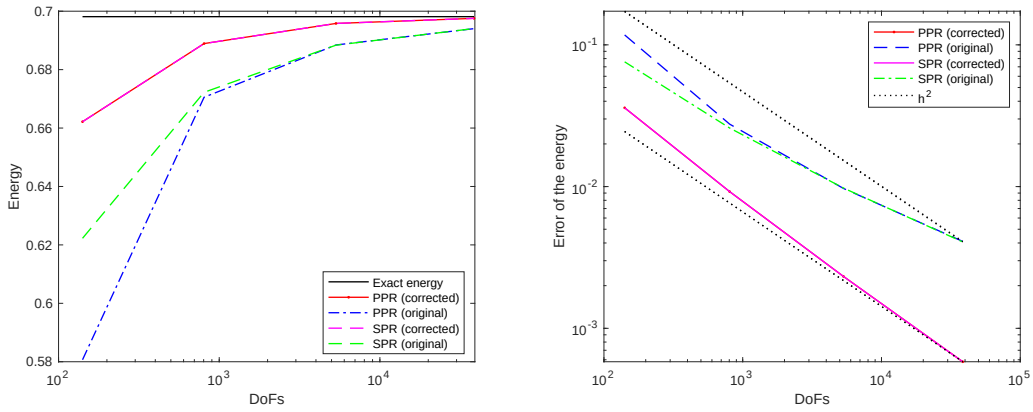

(a) (b)

Figure 6: The numerical convergence of the calculated demagnetizing field energy on a unit sphere with homogeneous magnetization $\vec{\mathrm{M}}(0,0,1)$. (a): The comparison of the demagnetizing field energy. (b): The comparison of the error.

5.2. Cases in a unit cube

In this subsection, two states of the magnetization field in a unit cube are considered, i.e., the homogeneous case and the vortex case, shown in Fig. 7.

5.2.1. Homogeneous magnetization

The homogeneous magnetization here is also $\vec{\mathrm{M}} = (0,0,1)$. Let $\Omega = [-0.5,0.5]^3$. In this case, demagnetizing field energy for the configuration is known as $1/6$, which can

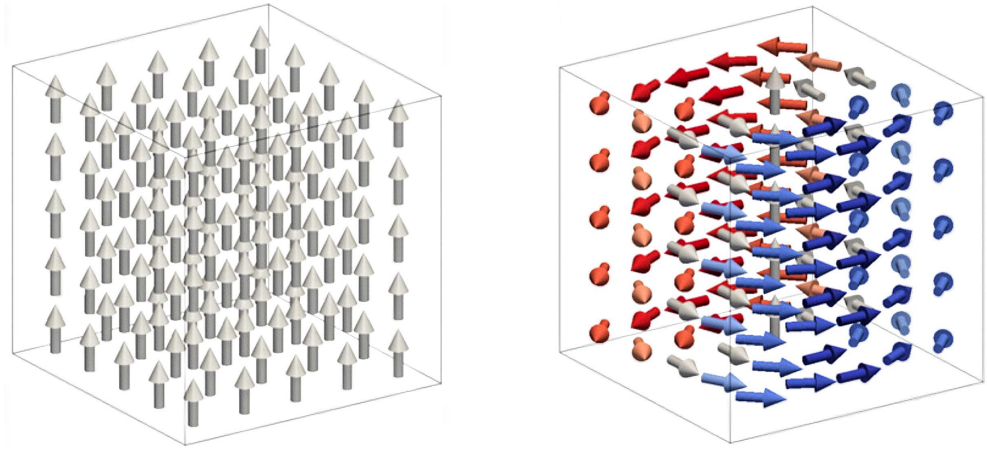

(a) (b)

Figure 7: Magnetization is on a $1 \times 1 \times 1$ cube. (a) homogeneous magnetization, (b) vortex state [1].

Table 2: The error and the convergence order for computing the E_{dem} by SPR and PPR technique.

Mesh(Dofs)	err_{SPR}	Order	err_{PPR}	Order
Cube0(365)	0.01001		0.01098	
Cube1(2457)	0.00424	1.3509	0.00415	1.5301
Cube2(17969)	0.00188	1.2246	0.00179	1.2706
Cube3(137313)	0.00087	1.1366	0.00083	1.125

be used as a reference value for checking the convergence. Table 2 shows the results for the demagnetizing field energy calculation using PPR and SPR with the original boundary integral.

Similar to observations from the previous subsection, it can be seen from Table 2 that results from SPR and PPR are comparable, due to the good configuration of the problem. Once again, the degeneration of the convergence order towards order 1 is also observed, which again confirms our theoretical results.

To show the effectiveness of the PPR technique, as well as the correction method we introduced, the behavior of the numerical solutions on the uniformly refined meshes is shown in Fig. 8. Two observations can be made from the results. From Fig. 8(a), with the refined surface mesh, the better approximate the demagnetizing field energy is obtained. It can also be observed that the PPR technique has a more precise result than the SPR technique wherever the method is with the corrected boundary integral or with the original boundary integral. Then the error, in Fig. 8(b), shows that the order of the convergence with the PPR technique under the corrected boundary integral has better behavior and has a tendency of a second-order convergence property.

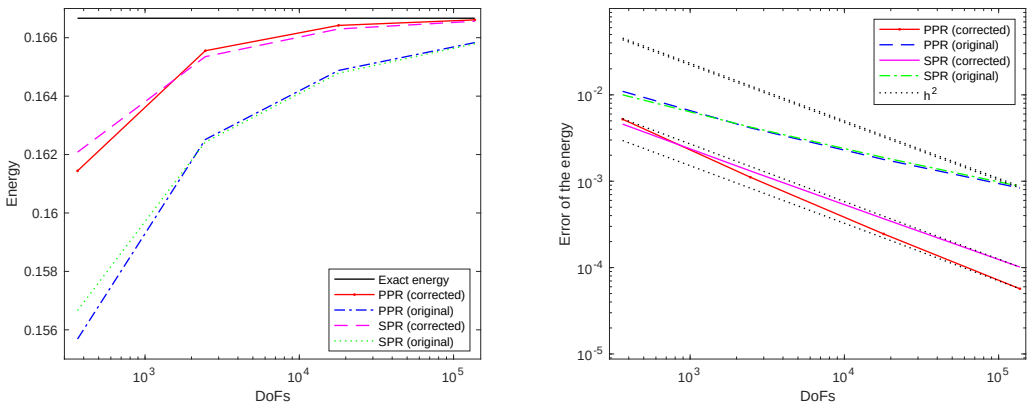

(a) (b)

Figure 8: The comparisons of the SPR and the PPR with the corrected boundary integral for the homogeneous magnetization $\vec{\mathrm{M}} = (0, 0, 1)$. (a): The comparison of the demagnetizing field energy. (b): The comparison of the error.

5.2.2. Vortex state

Let $\Omega = [-0.5, 0.5]^3$. Suppose that the magnetization is the one in the vortex state with $\vec{\mathrm{M}} = (m_x, m_y, m_z)$ given by

$$m_x = -\frac{y}{r}\left(1 - \exp\left(-4\frac{r^2}{r_c^2}\right)\right)^{1/2},$$
$$m_y = \frac{x}{r}\left(1 - \exp\left(-4\frac{r^2}{r_c^2}\right)\right)^{1/2},$$
$$m_z = \exp\left(-2\frac{r^2}{r_c^2}\right),$$

where $r = \sqrt{x^2 + y^2}$ and $r_c = 0.14$.

The configuration in this example is also discussed in [1]. In our work, we respectively use the approximate demagnetizing field energies for both the SPR technique (0.021774508) and the PPR technique (0.021787669) as the reference values, which are obtained on a mesh with 1073345 degrees of freedom.

From Table 3, the analysis in Section 2 is again confirmed that the accurate calculation of the boundary integral is essential for an optimal convergence. However, the feature of PPR on superior accuracy than SPR, which is not shown clearly in the previous two examples, can be observed well in this example. It can be seen that on all meshes, the numerical accuracy from PPR is better than that from SPR.

With the correction method proposed in the previous section, the demagnetizing field and corresponding energy are recalculated. From Fig. 9(a), it is obvious that the calculation of demagnetizing field energy with corrected boundary has an extremely expected result since we can get the approximate solution with less than 2500 mesh grids which the SPR technique cannot achieve, and also shows that the computational complexity could also be reduced by the PPR technique. Moreover, the performance of the SPR technique with the corrected boundary integral has similar behavior to the PPR technique with the initial boundary condition, which also shows the advantage of the PPR technique. From Fig. 9(b), the orders of the convergence with different approaches are shown. Both the techniques with better boundary integrals have better behaviors than that with original boundary integrals. After the first refined mesh, the PPR technique under the corrected boundary conditions has excellent superconvergence prop-

Table 3: The error and the convergence order for computing the E_{dem} on unit cube with vortex by SPR and PPR technique.

Mesh(Dofs)	err_{SPR}	Order	err_{PPR}	Order
Cube0(365)	0.00492		0.00296	
Cube1(2457)	0.00210	1.3408	0.00122	1.3912
Cube2(17969)	0.00089	1.2938	0.00064	0.9741
Cube3(137313)	0.00039	1.2277	0.00033	0.975

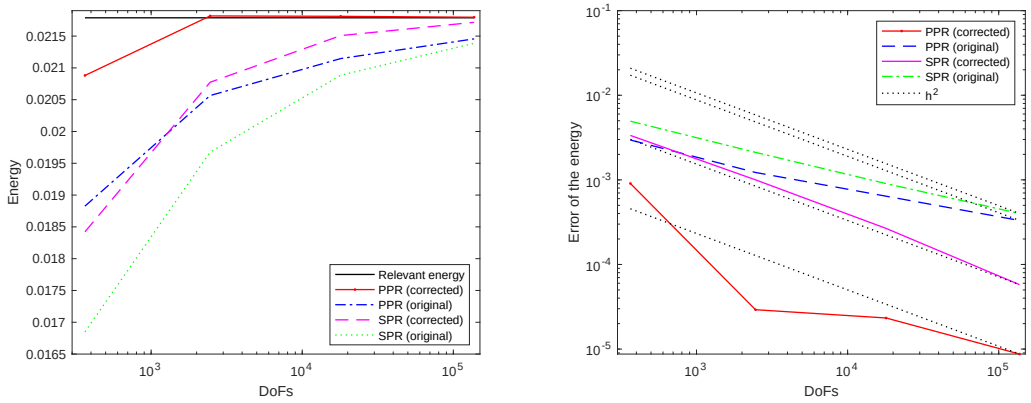

(a) (b)

Figure 9: The comparisons of the SPR and the PPR with the original and the corrected boundary integrals for the vortex. (a): The comparison of the demagnetizing field energy. (b): The comparison of the error.

erties. Even though the SPR method with the optimized boundary integrals has the expected order of the superconvergence, the PPR technique with corrected boundary integrals performs better. In addition, compared to the previous two cases, the PPR approach on challenging models with better approximation boundary conditions may have improved behavior.

6. Conclusion

In this paper, a gradient recovery method has been proposed for improving the accuracy of demagnetizing field calculation based on PDE approach, which has nearly second-order accuracy. The error estimate of the finite element solution and the superconvergence property of the PPR technique have been demonstrated theoretically and numerically. The locally refined surface meshes are offered exhaustively to compensate for the lack of information on the boundary integral, as indicated in the error estimates. The approach for developing the code for the numerical experiments is also detailed.

In the numerical experiments, the validity of the proposed work is tested numerically using examples on a unit sphere with homogenous magnetization, on a unit cube with homogenous magnetization and vortex state, as demonstrated in Sections 5.1 and 5.2. Numerical simulations on both simple and complicated domains proved the possibility of applying the suggested technology to actual problems. In addition, the PPR approach could be a quality candidate on dealing with challenging models with better approximation boundary conditions.

In our forthcoming work, the issue on the computational complexity of the demagnetizing field calculation will be discussed in depth, in which a treecode algorithm will be proposed to handle the boundary integral. In this case, an optimal complexity can be obtained. Together with the gradient recovery method proposed in this paper, an efficient solver for the demagnetizing field can be expected.

Acknowledgements

The authors would like to thank the anonymous reviewers for the valuable comments.

The research of Guanghui Hu is partially supported by the Science and Technology Development Fund, Macau SAR (Grant No. 0068/2024/RIA1), by the National Natural Science Foundation of China (No. 11922120), and by the MYRG of University of Macau (Grant No. MYRG-CRG2024-00042-FST). The research of Lei Yang is partially supported by the Science and Technology Development Fund, Macau SAR (Grant Nos. 0031/2022/A1, 0105/2024/RIB2).

References

[1] C. Abert, L. Exl, G. Selke, A. Drews, and T. Schrefl, *Numerical methods for the stray-field calculation: A comparison of recently developed algorithms*, J. Magn. Magn. Mater. 326 (2013), 176–185.

[2] C. Abert, G. Selke, B. Kruger, and A. Drews, *A fast finite-difference method for micromagnetics using the magnetic scalar potential*, IEEE Trans. Magn. 48(3) (2012), 1105–1109.

[3] R. Beatson and L. Greengard, *A short course on fast multipole methods*, Wavelets, multilevel methods and elliptic PDEs, 1 (1997), 1–37.

[4] J. Blue and M. R. Scheinfein, *Using multipoles decreases computation time for magnetostatic self-energy*, IEEE Trans. Magn. 27(6) (1991), 4778–4780.

[5] Z. Cai et al., *AFEPack: A general-purpose C++ library for numerical solutions of partial differential equations*, Commun. Comput. Phys. 36(1) (2024), 274–318.

[6] L. Caretta et al., *Fast current-driven domain walls and small skyrmions in a compensated ferrimagnet*, Nat. Nanotechnol. 13(12) (2018), 1154–1160.

[7] H. Chen, Z. Zhang, and Q. Zou, *A recovery based linear finite element method for 1D bi-harmonic problems*, J. Sci. Comput. 68 (2016), 375–394.

[8] J. Chen, D. Wang, and Q. Du, *Linear finite element superconvergence on simplicial meshes*, Math. Comput. 83(289) (2014), 2161–2185.

[9] L. Chen, *Superconvergence of tetrahedral linear finite elements*, Int. J. Numer. Anal. Model. 3(3) (2006), 273–282.

[10] Z. Chen and H. Wu, *Selected Topics in Finite Element Methods*, Science Press, (2010).

[11] P. G. Ciarlet, *The Finite Element Eethod for Elliptic Problems*, Classics in Applied Mathematics, SIAM (2002).

[12] J. De Klerk, *Effect of a magnetic field on the propagation of sound waves in a ferromagnetic material*, Nature 168 (1951), 963–964.

[13] Y. Du, H. Wu, and Z. Zhang, *Superconvergence analysis of linear FEM based on polynomial preserving recovery for Helmholtz equation with high wave number*, J. Comput. Appl. Math. 372 (2020), Paper No. 112731.

[14] D. R. Fredkin and T. R. Koehler, *Hybrid method for computing demagnetizing fields*, IEEE Trans. Magn. 26(2) (1990), 415–417.

[15] C. J. Garcia-Cervera and A. M. Roma, *Adaptive mesh refinement for micromagnetics simulations*, IEEE Trans. Magn. 42(6) (2006), 1648–1654.

[16] A. KNITTEL, M. FRANCHIN, G. BORDIGNON, T. FISCHBACHER, S. BENDING, AND H. FANGOHR, *Compression of boundary element matrix in micromagnetic simulations*, J. Appl. Phys. 105(7) (2009), Paper No. 07D542.

[17] J. LELIAERT, M. DVORNIK, J. MULKERS, J. DE CLERCQ, M. V. MILOŠEVIĆ, AND B. VAN WAEYENBERGE, *Fast micromagnetic simulations on GPU-recent advances made with mumax*^{3}, J. Phys. D: Appl. Phys. 51(12) (2018), Paper No. 123002.

[18] S. LEPADATU ET AL., *Synthetic ferrimagnet nanowires with very low critical current density for coupled domain wall motion*, Sci. Rep. 7(1) (2017), Paper No. 1640.

[19] H. LONG, E. T. ONG, Z. LIU, AND E. LI, *Fast Fourier transform on multipoles for rapid calculation of magnetostatic fields*, IEEE Trans. Magn. 42(2) (2006), 295–300.

[20] C. G. MAKRIDAKIS, *On the Babuška-Osborn approach to finite element analysis: L^2 estimates for unstructured meshes*, Numer. Math. 139(4) (2018), 831–844.

[21] A. NAGA AND Z. ZHANG, *A posteriori error estimates based on the polynomial preserving recovery*, SIAM J. Numer. Anal. 42(4) (2004), 1780–1800.

[22] A. NAGA AND Z. ZHANG, *A new finite element gradient recovery method: Superconvergence property*, SIAM J. Sci. Comput. 26(4) (2005), 1192–1213.

[23] A. NAGA AND Z. ZHANG, *The polynomial-preserving recovery for higher order finite element methods in 2D and 3D*, Discrete Contin. Dyn. Syst.-B 5(3) (2005), 769–798.

[24] S. REIMERS ET AL., *Defect-driven antiferromagnetic domain walls in CuMnAs films*, Nat. Commun. 13(1) (2022), Paper No. 724.

[25] T. SCHREFL, *Finite elements in numerical micromagnetics: Part II: Patterned magnetic elements*, J. Magn. Magn. Mater. 207(1) (1999), 66–77.

[26] T. SCHREFL, J. FIDLER, K. J. KIRK, AND J. N. CHAPMAN, *A higher order FEM-BEM method for the calculation of domain processes in magnetic nano-elements*, IEEE Trans. Magn. 33(5) (2002), 4182–4184.

[27] J. XU AND Z. ZHANG, *Analysis of recovery type a posteriori error estimators for mildly structured grids*, Math. Comput. 73(247) (2004), 1139–1152.

[28] L. YANG, J. CHEN, AND G. HU, *A framework of the finite element solution of the Landau-Lifshitz-Gilbert equation on tetrahedral meshes*, J. Comput. Phys. 431 (2021), Paper No. 110142.

[29] L. YANG AND G. HU, *An adaptive finite element solver for demagnetization field calculation*, Adv. Appl. Math. Mech. 11 (2019), 1048–1063.

[30] O. C. ZIENKIEWICZ AND J. Z. ZHU, *The superconvergent patch recovery and a posteriori error estimates. Part 1: The recovery technique*, Int. J. Numer. Methods Eng. 33(7) (1992), 1331–1364.